Effect of bank curvatures on hyporheic water exchange at meter scale

Guotao Zhang, Jinxi Song, Ming Wen, Junlong Zhang, Weiwei Jiang, Liping Wang, Feihe Kong and Yuanyuan Wang

ABSTRACT

The micro-topography feature of a riverine system is a controlling attribute to induce the change of patterns and magnitudes of hyporheic water exchange. The study aims to determine how hyporheic water exchange is affected by the bank curvatures of test points at meter scale. A one-dimensional heat steady-state transport model was applied to determine patterns and magnitudes of vertical hyporheic water exchange in January and July 2015. The bank curvatures were calculated based on the curvature formula. The results demonstrate that vertical water exchange patterns of all test points were upwards during the two test periods, and the higher vertical fluxes mostly occurred in January 2015. Large curvatures for either sides of convex banks in the two periods resulted in higher vertical water exchange fluxes, and the significantly higher vertical fluxes occurred near the apex of bends. Additionally, a flow pattern from river bank discharging into stream was derived during the campaign in July 2015, and significantly higher fluxes were obtained along the straight bank where more riparian vegetation was adjacent to the bank/water interface. It can be suggested that the bank curvatures and riparian vegetation are considered the crucial attributes influencing hyporheic water exchange.

Key words | curvatures, hyporheic water exchange, riparian vegetation, temperature distribution, Weihe River

Guotao Zhang
Jinxi Song (corresponding author)
Ming Wen
Junlong Zhang
Weiwei Jiang
Liping Wang
Feihe Kong
Yuanyuan Wang
College of Urban and Environmental Sciences,
Northwest University,
Xi'an 710127,
China
E-mail: *jinxisong@nwu.edu.cn*

Jinxi Song
State Key Laboratory of Soil Erosion and Dryland Farming on the Loess Plateau,
Institute of Soil and Water Conservation, Chinese Academy of Sciences,
Yangling 712100,
China

INTRODUCTION

Interactions between surface water and groundwater mainly occur in or across the hyporheic zone (HZ), which plays a pivotal role in hydrology discipline (Krause *et al.* 2009). The HZ is regarded as the saturated transition zone and the active ecotone between groundwater and the surface water body (Cheng *et al.* 2015). Hyporheic water exchange is the movement of water that infiltrates and flows through the streambed and adjacent aquifer, and returns to the surface water after a short period of residence (Cranswick *et al.* 2014), influencing and regulating the physical and biochemical transport processes (Revelli *et al.* 2008; Song *et al.* 2015b). Hence, accurate estimation of the hyporheic water exchange processes is essential to evaluate the fate and transport of the contaminants as well as the health of aquatic biota in aquifer systems, which is significant for water resources management and aquatic habitat investigations (Wörman *et al.* 2002; Boano *et al.* 2007; Datry *et al.* 2007; Zuo *et al.* 2014). However, hyporheic flow through the deposition environment is, to some extent, driven by topography features along the river bank or the riverbed (Boano *et al.* 2006; Cardenas 2009; Stonedahl *et al.* 2013; Cai *et al.* 2015), thus augmenting the difficulty of understanding the hyporheic water exchange processes.

The dynamics of hyporheic water exchange are easily caused by different topographic features including riverbed slope and bed forms (Cardenas & Wilson 2006; Boano *et al.* 2007; Jin *et al.* 2011), land surface topography (Wörman *et al.* 2006), and channel bars and meandering

doi: 10.2166/nh.2016.046

stream channels (Boano *et al.* 2007; Stonedahl *et al.* 2013; Boyraz & Kazezyılmaz-Alhan 2014; Jiang *et al.* 2015). These topography features can further alter or change the patterns and magnitudes of hyporheic water exchange. It has been shown that topographic features, including a fluvial island, the streambed and the adjacent stream bank are the crucial influencing factors of hyporheic water exchange and biochemical transport processes (Jin *et al.* 2010; Shope *et al.* 2012; Gomez-Velez *et al.* 2015). However, scales and dimensions of topography are the pivotal factors influencing patterns and magnitudes of hyporheic water exchange (Stonedahl *et al.* 2010; Cranswick & Cook 2015). The relations between different sinuosities along the stream and hyporheic water fluxes in field sites are presented by simulating the morphodynamic evolution of meandering rivers at different scales (Revelli *et al.* 2008). In addition, either small or large scales of topography between ripples and meanders have some significant influences on hyporheic flow fields and residence time distributions (Stonedahl *et al.* 2010). Furthermore, the HZ near the apex of bends along the bank at large scale can be maintained well even under gaining or losing conditions (Cardenas 2009). However, for small scale, what hyporheic water exchange is and how the bank curvatures influence hyporheic water exchange are still unknown. In this study, the hyporheic water exchange along the meandering bank at meter scale is investigated and the effects of bank curvatures on hyporheic water exchange are demonstrated.

The hyporheic water exchange can be measured by several methods including head piezometers (Nowinski *et al.* 2011), seepage meters (Zhu *et al.* 2015), differential discharge gauging (Lowry *et al.* 2007), the thermal method (Schmidt *et al.* 2006; Shope *et al.* 2012; Anibas *et al.* 2015) and other methods (Carey & Quinton 2005; Wei *et al.* 2012; Li *et al.* 2015). Hatch *et al.* (2006) presented a table to summarize the characteristics of several methods, and regarded heat as an important natural tracer for identification and quantification of hyporheic water exchange. The thermal method is very effective to evaluate the magnitudes and patterns of hyporheic water exchange, and is fast, adjustable, and relatively inexpensive as well as accurate for temperature measurement. Additionally, water exchange fluxes in the HZ can be inferred quantitatively from convective processes or determined by the temperature gradient profiles of the streambed (Kalbus *et al.* 2006; Schmidt *et al.* 2007; Anibas *et al.* 2011; Naranjo & Turcotte 2015). Numerical models at different spatial scales are increasingly utilized to elucidate the dynamic processes of hyporheic water exchange in controlled scenario simulations (Fleckenstein *et al.* 2010; Shope *et al.* 2012; Anibas *et al.* 2015), and to address the effects of several topography features on hyporheic water exchange (Fanelli & Lautz 2008; Shope *et al.* 2012; Schmidt *et al.* 2014; Cranswick & Cook 2015). One-dimensional heat transport model (Suzuki 1960; Stallman 1965) was applied to assess the temporal and spatial distribution of surface water and groundwater interactions at different scales (Anderson 2005; Anibas *et al.* 2012). On the basis of the steady-state thermal assumption, a one-dimensional heat steady-state model, presented by Schmidt *et al.* (2006) and validated by Anibas *et al.* (2009), is able to evaluate the hyporheic water exchange with sufficient temporal and spatial resolution.

Thus, the one-dimensional heat steady-state model is applied to estimate the vertical hyporheic water exchange along the meandering bank at meter scale in the Weihe River, and the bank curvatures are measured as well. The objective of this study is: (1) to illustrate the patterns and magnitudes of vertical hyporheic water exchange at different points along the meandering bank; and (2) to demonstrate the effect of bank curvatures on vertical hyporheic water exchange at meter scale.

STUDY AREA AND METHODS

Study area

The study area (N34 °22′28.63″, E108 °50′01.70″) is located along the Weihe River, Xi'an City, Shaanxi Province, China (Figure 1). The Weihe River, as the largest tributary of the Yellow River, has a total length of approximately 818 km and a drainage area of about 1.34×10^5 km^2. It originates from Niaoshu Mountain in Gansu Province, and flows into the Yellow River at Tongguan County in Shaanxi Province. The Weihe River basin has an arid and semi-arid climate with an annual average temperature of approximately 13.3 °C. The annual rainfall in the river basin is 558–750 mm, with a gradually increasing trend from north

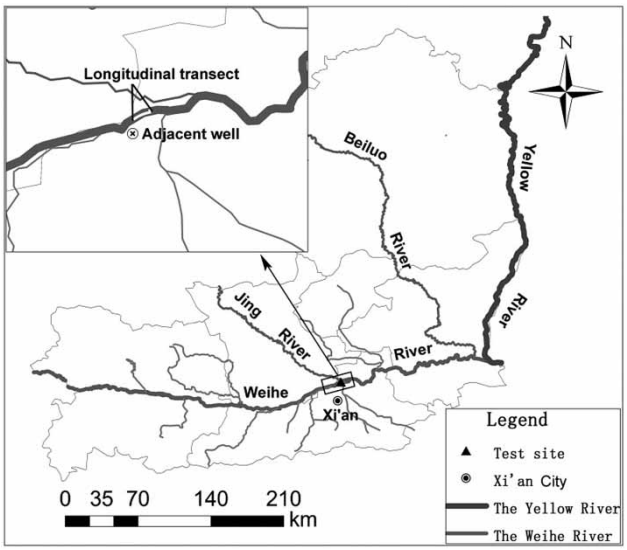

Figure 1 | Map of the study area, showing the location of test sites in the catchment.

to south. About 60% of the annual precipitation is concentrated in the flood season of May to September. In addition, the river basin is mostly covered with loose loess, which can result in heavy sediment transport and serious siltation in the river channel.

In the study area, the left bank along the flow direction is an erosional bank while the right bank is a depositional bank (Figure 2(a)). During the campaign in January 2015, a total of 18 tests were conducted along the meandering right bank with a length of 180 m, which could be divided into three sections including two convex banks (CB_1 and CB_2) as well as one depositional area (DA) (Figure 3(a) and Table 1). The mean value of water depth from test points was approximately 0.15 m, and the river width ranged from 136 to 160 m. The longitudinal slope was 0.167‰ and the direction of water flow was east-north east (ENE). The meandering bank induced sediment erosion and deposition from flood. The materials in the streambed sediment along CB_1 and CB_2 contained mostly fine sand. The sediment materials along the DA consisted of silt deposition in the upper layer and fine sand and gravel in the lower layer of vertical layers 0.80 m depth.

The practical datasets of micro-topography and temperature along the meandering right bank, including two segmentations of straight bank (SB_1 and SB_2) and one convex bank (CB_3), were collected near the former site in July 2015 (Figure 3(b) and Table 1). Summer and winter in the thermal steady-state investigation are regarded as the two most favorable seasons when the steady temperature distributions are formed in streambed sediment (Schmidt *et al.* 2006; Anibas *et al.* 2009). The sediment temperature distributions of different test points could be applied to analyze the influence of bank curvatures on water exchange in the HZ. The riparian vegetation has some significant influence on hyporheic water exchange (Brunke & Gonser 1997; Anibas *et al.* 2012; Tan *et al.* 2016). Along the straight bank

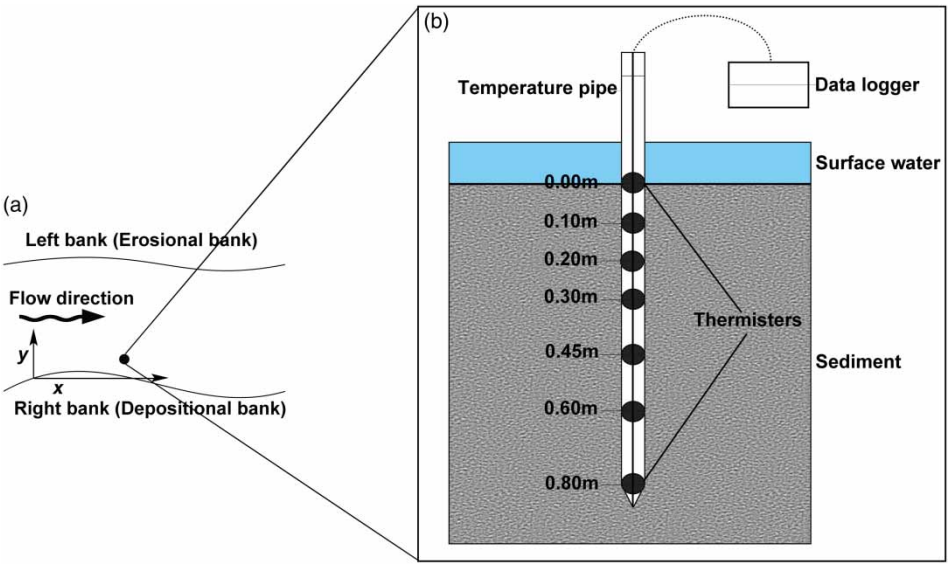

Figure 2 | Schematic diagrams of the locations of test points close to the right bank in the Weihe River, indicating the sediment erosion and deposition along the bank (a), and measurement setup of temperature distributions in streambed sediment with the temperature pipe (b).

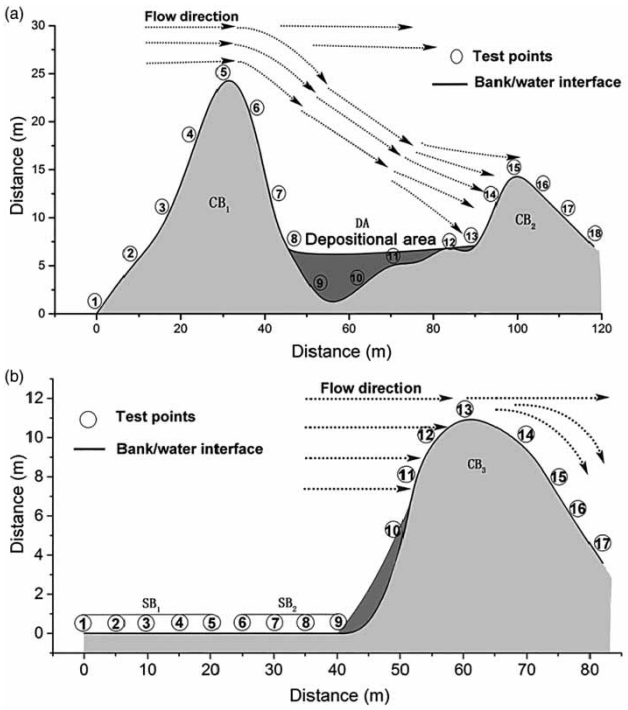

Figure 3 | Test sites showing the three divided sections along the bank in January 2015 (a) CB_1, AD, CB_2 and three other divided sections along the bank in July 2015 (b) SB_1, SB_2, CB_3. (The *x*-axis is the distance from the first test point on the bank along the flow direction; the *y*-axis is the perpendicular distance from the test site point to the *x*-axis.)

segmentations (SB_1 and SB_2), the riparian vegetation with two areas of $15 \times 15\ m^2$ were investigated, which included coverage rates and major floristics of arbor, shrub, and herb adjacent to the bank/water interface (Table 2). The major floristics in the two areas was almost similar, containing *Gramineae* and *Compositae*, *Oleander* as well as *Willow*. However, the riparian vegetation in SB_1 accounted for larger coverage rates, and was significantly closer to the bank/water interface in comparison to the vegetation in SB_2.

METHODS

Temperature measurement

Along the meandering bank, a 2.0 m manual instrument equipped with seven thermistors at definite depths was pressed into the sediment to monitor the temperatures of seven sediment layers (including 0.00 m, 0.10 m, 0.20 m, 0.30 m, 0.45 m, 0.60 m, 0.80 m) (Figure 2(b)). Once the pipe was inserted into the sediment, the sensors started to work. The temperature signals of different depths in the streambed sediment were transmitted to a data logger with logging and storage functions. In order to eliminate the effects of thermal conduction on the temperatures of different depths, the test was done at least at 15 min intervals for each measurement until the temperature reached a steady state. In addition, to accurately obtain the temperature signals, the device needed to be adjusted and calibrated before and after deployment with an error of $\pm 0.05\ ^{\circ}C$. All test points in the longitudinal flow direction were done at 5–10 m spacing based on the topography along the river bank, and those in the lateral direction were approximately 1.0 m away from the bank/water interface (Figure 3).

Determination of patterns and magnitudes of hyporheic water exchange

Taking into consideration both convection and conductive transports, a one-dimensional heat transport model (Equation (1)) was applied to calculate the magnitudes of water exchange fluxes between surface water and groundwater. The prerequisites are the underlying hypothesis that water flow in the streambed is vertical (e.g., in the z

Table 1 | Evaluations of different sections along the bank in the Weihe River in January and July 2015

Sections	Test points	Ranges of flux (mm d^{-1})	Mean flux (mm d^{-1})	Standard deviation of flux	Largest curvature (m^{-1})	Mean velocity (m/s)
CB_1	1–9	19.59–78.81	49.15	22.43	0.18	0.54
DA	10–12	58.83–81.12	67.81	11.76	–*	0.34
CB_2	13–18	32.91–72.52	52.74	13.27	0.05	0.40
SB_1	1–5	24.57–27.21	25.89	1.02	0	0.31
SB_2	6–9	31.85–34.44	32.40	1.22	0	0.30
CB_3	10–17	18.03–27.63	23.30	4.28	0.08	0.25

*Indicating no data obtained due to uncertainty of changeable bending induced by the depositional processes.

Table 2 | Riparian vegetation distributions along the straight bank segmentations in July 2015

Sections	SB_1						SB_2			
Test points		1	2	3	4	5	6	7	8	9
Distance (m)*		6.7	7.1	6.5	6.1	6.1	1.3	0.6	2.6	2.3
Coverage rates (%)	Herb	60					80			
	Shrub	8.2					10.5			
	Arbor	1.5					6.5			
Major floristics	Herb	*Gramineae* and *Compositae*					*Gramineae* and *Compositae*			
	Shrub	*Oleander*					*Oleander*			
	Arbor	*Willow*					*Willow*			

*Indicating the measured distances from the riparian vegetation boundary to the bank/water interface.

direction, $x = 0$, $y = 0$) and the materials of the streambed are the natural saturated, porous, homogeneous media (Schmidt *et al.* 2006):

$$\frac{\partial T(z)}{\partial t} = \frac{K_{fs}}{\rho c}\nabla^2 T(z) - \frac{\rho_f c_f}{\rho c}\nabla(T(z)q_z) \tag{1}$$

$$\rho c = n\rho_f c_f + (1-n)\rho_s c_s \tag{2}$$

where $T(z)$ is the riverbed temperature at depth z at time t (°C); $\rho_f c_f$, $\rho_s c_s$, and ρc are the volumetric heat capacity of fluid, solid, and solid-fluid system (J m^{-3} k^{-1}), respectively; n is porosity of the porous saturated media; K_{fs} is thermal conductivity of the solid–fluid matrix (J s^{-1} m^{-1} k^{-1}); q_z is the specific discharge or flow velocity in the vertical (z) direction (m s^{-1}). For the sake of convenience, q_z is generally expressed with the unit mm d^{-1}.

An underlying assumption is that the water flows are required to be upward in the vertical (z) direction, which is appropriate for the gaining area (e.g., upward flow) in the study site. Under the thermal steady-state conditions, the temperature variations of streambed sediment in the aquifer domain always tend to be constant during the measurement period, equivalent with $\partial T/\partial t \to 0$. Thus, it is a good approximation to treat it as zero, and expressed as follows (Anibas *et al.* 2011):

$$\frac{\partial T(z)}{\partial t} = \frac{K_{fs}}{\rho c}\nabla^2 T(z) - \frac{\rho_f c_f}{\rho c}\nabla(T(z)q_z) = 0 \tag{3}$$

The upper condition $T = T_0$ (°C) for the $z = 0$ and the lower boundary condition $T = T_L$ (°C) for the $z = L$ are provided (Schmidt *et al.* 2007) (Figure 4), and the analytical solution is given as follows:

$$\frac{T(z) - T_L}{T_0 - T_L} = \exp\left(-q_z \frac{\rho_f c_f}{k_{fs}}\right) \tag{4}$$

Additionally, Equation (4) can be adjusted and rearranged to obtain the following equation (Schmidt *et al.* 2007):

$$q_z = -\frac{K_{fs}}{\rho_f c_f z}\ln\frac{T(z) - T_L}{T_0 - T_L} \tag{5}$$

The one-dimensional heat steady-state transport model (Equation (5)) is undertaken using the parameters in January and July 2015 shown in Table 3, which can be directly applied to calculate the magnitudes of vertical hyporheic water exchange fluxes. The heat capacity of water (c_f) and thermal conductivity (K_{fs}) are obtained by applying measured sediment and water samples. As well, the upper and lower boundary conditions are also significant (Yuan *et al.* 2008), and have been determined (Table 3) (Schmidt *et al.* 2007). T_0, as the upper boundary condition, is the temperature value at 0.00 m depth (e.g., the interface between stream and streambed sediment). T_L, as the lower boundary condition, is a measured groundwater temperature value of a well close to the stream in the test site. Therefore, the input parameters of the physical properties and boundary conditions during two test periods are determined for the one-dimensional heat steady-state transport model to estimate the magnitudes of vertical hyporheic water exchange (Table 3).

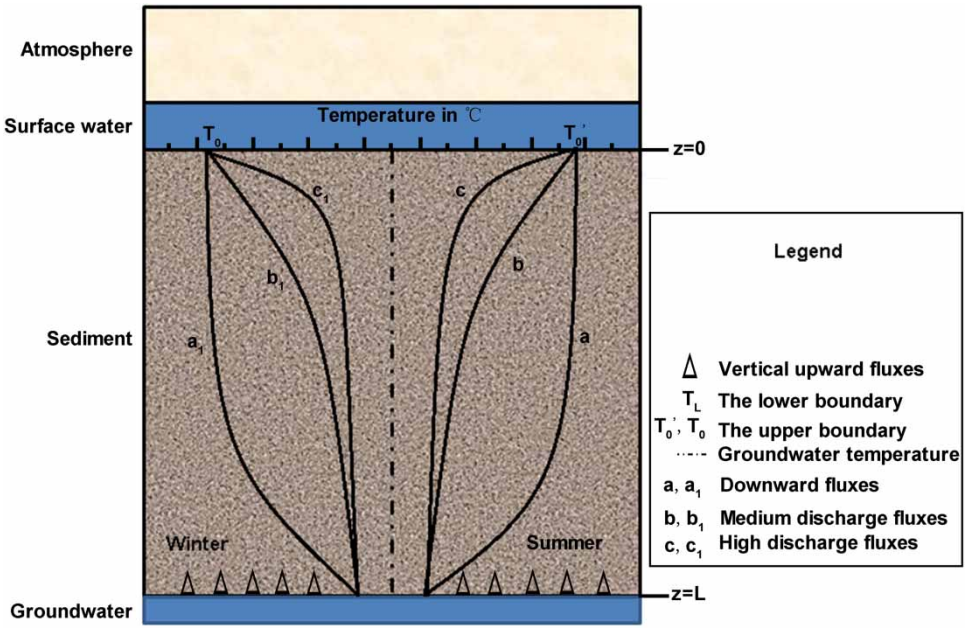

Figure 4 | Schematic of vertical temperature profiles for one-dimensional heat and water transport in a streambed based on the thermal steady-state conditions in winter and summer seasons: a, b, c show the vertical water fluxes in summer; a_1, b_1, c_1 show the vertical water fluxes in winter (modified from Anibas *et al.* (2011)).

Table 3 | Input parameters for determining the physical properties and boundary conditions for one-dimensional heat steady-state transport model (Equation (5))

Parameters	Values (winter)	Values (summer)	Units
Thermal conductivity, K_{fs}	1.695	1.765	J s^{-1} m^{-1} k^{-1}
Heat capacity of water, c_f	4,223	4,224	J kg^{-1} K^{-1}
Density of water, ρ_f	1,000	1,000	Kg m^{-3}
Upper boundary condition, T_0[a]	5.2	27.7	°C
Lower boundary condition, T_L[b]	11.3	11.8	°C

[a]Located at the interface (0.00 m) between surface water and streambed.
[b]Located at 10.5 m depth below the interface between surface water and streambed.

Additionally, on the basis of the upper and lower boundary conditions, the patterns (upward and downward) of hyporheic water exchange can be indicated by fitting the temperature distributions at multiple depths to the fitting curves (Figure 4). The temperatures include the temperature of surface water and streambed sediment, as well as groundwater. When the groundwater flow is upward and discharges into the surface water, the temperature profiles are convex upward with the high discharge fluxes (Figure 4 (c and c_1)) and medium discharge fluxes (Figure 4 (b and b_1)). Likewise, temperature profiles are concave upward under the circumstances that water flow is downward and recharges into groundwater (Figure 4 (a and a_1)).

Calculation of bank curvatures

For the sake of feasibility, the bank/water interface is determined based on simulated estimation of bending shape by establishing the coordinate system in test sites (Figure 5). The x-axis is the distance from the first test point on the bank along the flow direction, while the y-axis is the perpendicular distance from the test site point to the x-axis. Accordingly, the three convex banks (CB_1, CB_2, and CB_3) are simulated and corresponding fitting mathematical equations are obtained such that:

$$y_1 = -0.0023x^3 + 0.135x^2 - 1.5693x + 9.8619 \ (R^2 = 0.9808) \quad (6)$$

$$y_2 = -0.0285x^2 + 5.8516x - 286.85 \ (R^2 = 0.9619) \quad (7)$$

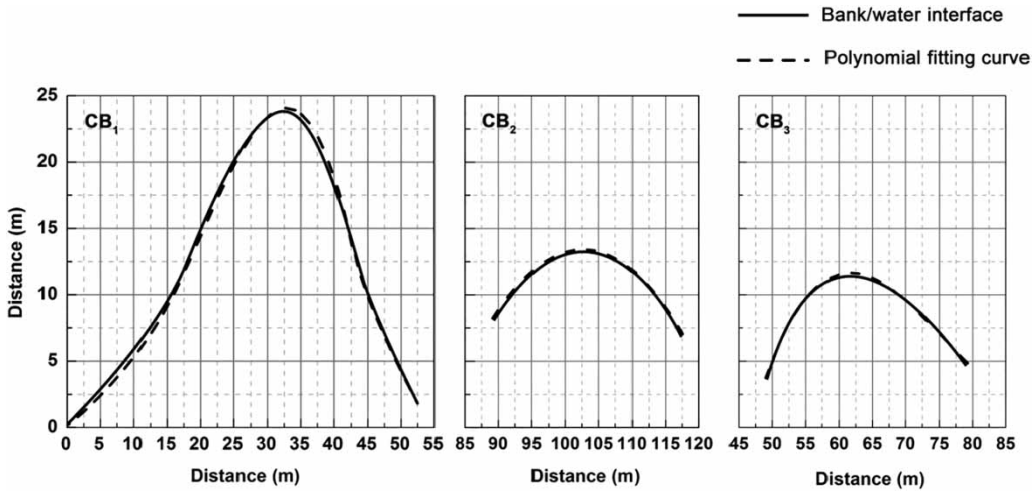

Figure 5 | The polynomial fitting curves for two convex banks in January 2015 (CB_1, CB_2) and one convex bank in July 2015 (CB_3). The solid line indicates the bank/water interface along the meandering banks; the dashed line indicates the polynomial fitting curve for the bank/water interface.

$$y_3 = 0.0009x^3 - 0.204x^2 + 14.912x - 342.86 \quad (R^2 = 0.9985) \tag{8}$$

where y_1, y_2, y_3 represent the fitting mathematical equations for CB_1, CB_2, and CB_3 respectively, practically reflecting the bending shape of the meandering banks (Figure 5). The alluvial meandering banks were investigated taking into account site- and time-specific factors; and only the method obtaining the mathematical equations, but not the actual equations, could be applied at other test sites. Simultaneously on the basis of Equations (6)–(8) as well as curvature formula Equation (9), the curvatures of test points along the banks are calculated. The curvature formula is expressed as follows:

$$\theta = y''/\left(1 + y'^2\right)^{3/2} \tag{9}$$

where θ is the curvatures of different test points along the meandering banks (e.g., $\theta = 1/r$, r indicates the curvature radius (Bai 2012)). y', y'' are the first derivative and second derivative of y function, respectively.

According to the variations of bank curvatures, the corresponding test points along the meandering bank were conducted during the two campaigns in January and July 2015. Applying Equations (5) and (9), the effects of curvatures of different test points on vertical hyporheic water exchange are elucidated in detail, which can be used to indicate the driving forces of water exchange in HZ.

RESULTS AND DISCUSSION

Patterns and magnitudes of hyporheic water exchange

According to the analyses of temperature distributions of streambed sediment from *in situ* tests, the vertical hyporheic water exchange patterns were determined along the banks in January and July 2015 (Figure 6). The temperature profiles in streambed sediment indicated that the patterns of vertical hyporheic water exchange were upward for all test sites during the two test periods (Figure 6). The significant variations of temperature profiles in the sediment domain occurred at the depth of 0.00–0.20 m (Figure 6(a) and 6(b)), which could be an active layer of hyporheic water exchange during the campaign in January 2015. However, the bending degrees of different temperature profiles are proportional to the hyporheic water exchange fluxes (Arriaga & Leap 2004), but do not accurately quantify the water exchange fluxes. On the basis of Equation (5), the magnitudes of vertical water exchange fluxes were estimated to range from 19.59 to 81.12 mm d^{-1} in January 2015 and from 18.03 mm d^{-1} to 34.44 mm d^{-1} in July 2015, respectively (Figures 7(b) and 8(b)). These values were higher

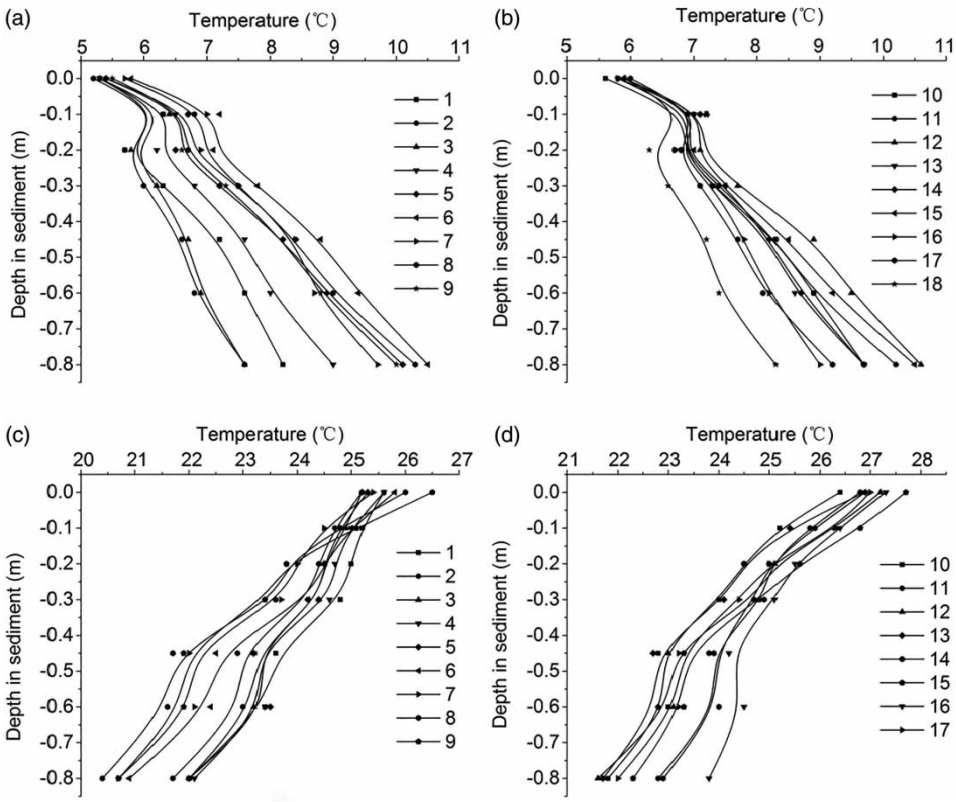

Figure 6 | Temperature profiles measured in streambed sediment along the bank in January 2015 (a), (b) and in July 2015 (c), (d).

than the 10 mm d^{-1} magnitude of upward hyporheic water exchange fluxes reported by Storey *et al.* (2003) and Schmidt *et al.* (2006), which further indicates the significant upward hyporheic flow of all test points.

The mean magnitude of hyporheic water exchange from 18 test points in January 2015 was 53.4 mm d^{-1}, which was approximately two times greater than the mean flux of 25.5 mm d^{-1} from 17 test points in July 2015 (Figures 7(b) and 8(b)). Mostly, the magnitude of vertical hyporheic water exchange for individual test points was higher in January 2015 than that in July 2015, which was analogous to the results of the Aa River in Belgium from Anibas *et al.* (2011). This might be caused by the significant variation of instream flow along with occurrence of the dry season in winter and wet season in summer. In addition, for every section during the two test periods, standard deviations (Table 1) indicated the different discrete degree of the magnitudes of vertical hyporheic water exchange for all test points. Compared to the straight banks (SB_1 and SB_2), the larger discrete degree of vertical water exchange fluxes occurred in the convex banks (CB_1, CB_2, and CB_3) (Table 1). However, in SB_1 and SB_2, the magnitudes of vertical hyporheic water exchange with the low discrete degree were always the same. It may possibly be affected by microtopography along the meandering bank.

Evaluation of curvatures for the different test points along the bank

The significant differences of temperature distributions are illustrated in the isothermal diagrams of sectional drawings in Figures 7(a) and 8(a). Moreover, the temperature distribution and vertical water exchange fluxes of streambed sediment near the apex of bends are strikingly varied (Figures 7 and 8). Anibas *et al.* (2011) indicated temperature distributions were affected by the underlying uneven geometry of river cross-sections due to the curvature in light of isothermal diagrams along the longitudinal cross-section of the river centerline. However, the curvature along the bank, as the driving force of hyporheic water exchange,

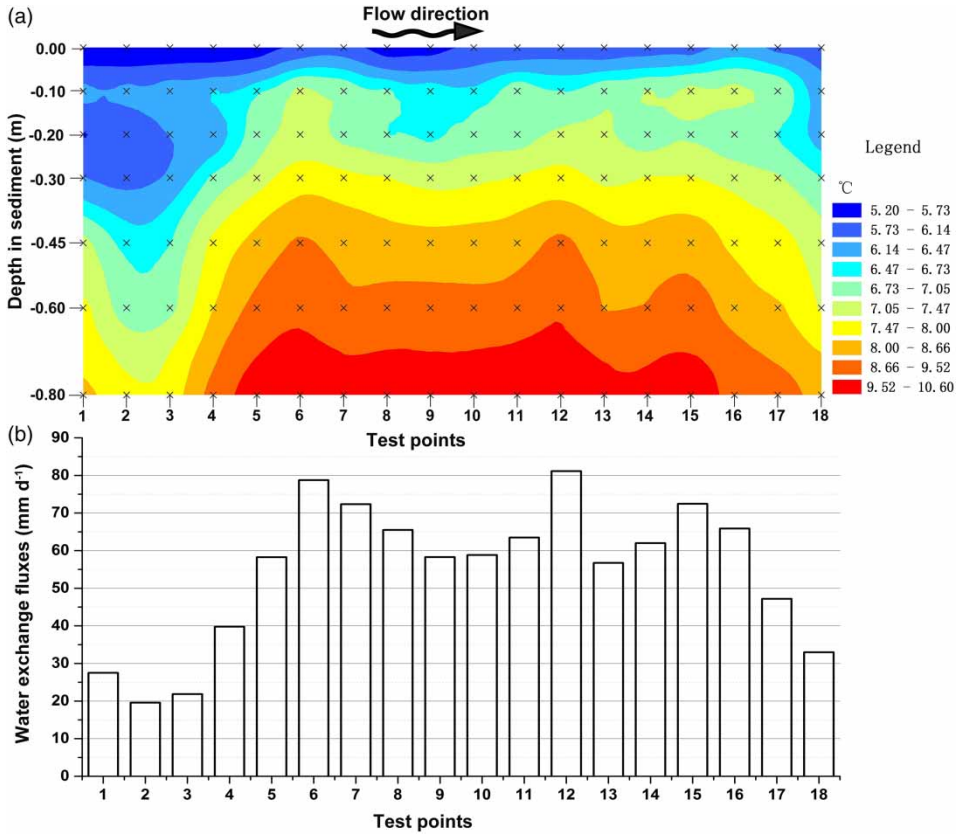

Figure 7 | Temperature distributions and hyporheic water exchange fluxes in January 2015. (a) Diagrammatical sectional drawings of temperature spatial distributions in streambed sediment along the meandering bank. (b) Bar graph depicting the magnitudes of hyporheic water exchange fluxes at different test points.

should be investigated to determine the influencing extent of integrated sinuosity on patterns and magnitudes of hyporheic water exchange (Boano *et al.* 2006; Revelli *et al.* 2008).

Along the meandering banks at meter scale, the curvatures of different test points in January and July 2015 were calculated and applied to analyze their influences on vertical hyporheic water exchange. In particular, the positive correlation of both curvatures and water exchange fluxes is illustrated along the three convex banks (CB_1, CB_2, and CB_3). The correlation coefficients are 0.601 (CB_1), 0.755 (CB_2, $p < 0.05$), and 0.733 (CB_3, $p < 0.05$) (Figure 9(a), 9(b), and 9(d)). On account of possible comprehensive effects of curvatures and riparian vegetation adjacent to the bank/water interface, these test points (including 1 and 2 in CB_1 and 10 and 17 in $CB_{3,}$) are excluded. Compared with the curvatures of different test points along either side of the convex bank, larger curvatures among the test points were inclined to induce a higher magnitude of vertical hyporheic water exchange fluxes. In terms of every convex bank, the highest magnitude of vertical fluxes occurred in the apex of bends with the greatest value of curvatures (Figure 9), which were significantly higher than the fluxes in other test points along the convex bank (Table 1). In addition, the finding of higher vertical water exchange fluxes occurring near the bends' apex was similar to the results reported by Cardenas (2009) in the USA.

Due to uncertainty of changeable bending induced by the depositional processes, no available data could be obtained to express curvatures for the DA in January 2015. The DA was gradually formed by a decreasing of stream flow from the upstream CB_1 (Figure 3(a)). Comparing mean values of vertical hyporheic water flux of test points in DA with that of other test points along the bank, it could be found that the extent of vertical hyporheic water exchange increased with sediment deposition (Figure 7(b) and Table 1). The sediment materials in the DA consisted of silt deposition of the upper layer and

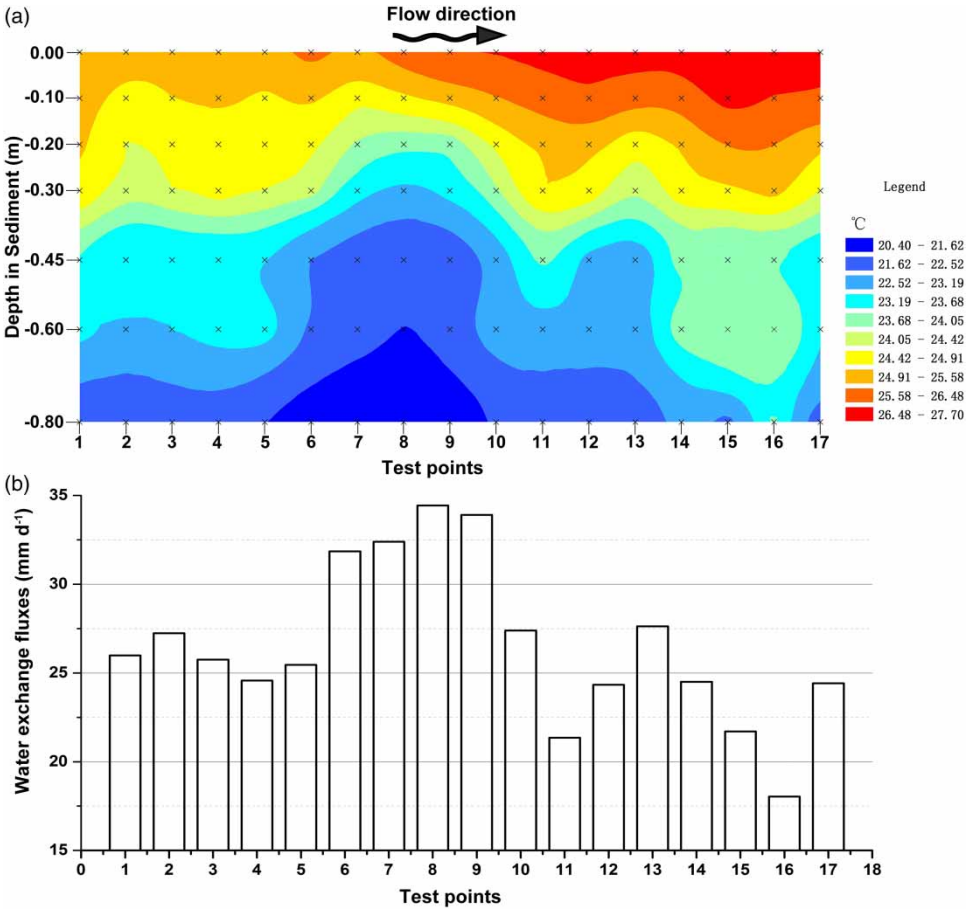

Figure 8 | Temperature distributions and hyporheic water exchange fluxes in July 2015. (a) Diagrammatical sectional drawings of temperature spatial distributions in streambed sediment along the meandering bank. (b) Bar graph depicting the magnitudes of hyporheic water exchange fluxes at different test points.

fine sand and gravel of the lower layer. It presented a larger heterogeneity within the vertical layer of streambed sediment, which was induced and further magnified by the bank curvatures. This heterogeneity could give rise to the significant additional water exchange fluxes in comparison to the equivalent homogenous media (Cardenas *et al.* 2004). Moreover, the integrated meandering river bank, formed by the sediment erosion and deposition, could cause the variation of hydraulic gradient and further generate the different water exchange fluxes (Jiang *et al.* 2015; Şahin & Çiftçi 2016). In this study, the erosion and deposition locations along the meandering bank at meter scale differed from those in the meandering stream channel at large scales (Malard *et al.* 2002; Anibas *et al.* 2011) (Figure 3). This indicated that the small scales of erosion and deposition locations' variation had a great effect on vertical hyporheic water exchange.

The isothermal diagrams of sectional drawings illustrate the difference of temperature distributions within a depth of 0.00–0.80 m for streambed sediment in test points during the two campaigns (Figures 7(a) and 8(a)). Especially, the greater change of temperature distributions and vertical hyporheic water fluxes occurred at the three convex banks (CB_1, CB_2, and CB_3) (Figures 7(a) and 8(a)). During the winter, the temperature is colder in surface water than in groundwater, whereas generally it is the opposite in summer. The significantly high temperature in winter and low temperature in summer of the test layers in streambed sediment mostly occurred near the bends' apex with the large curvatures, where the higher hyporheic water exchange occurred (Figures 7 and 8). Meanwhile, along either side of every convex bank, the streambed sediment of test points indicated strikingly regular temperature

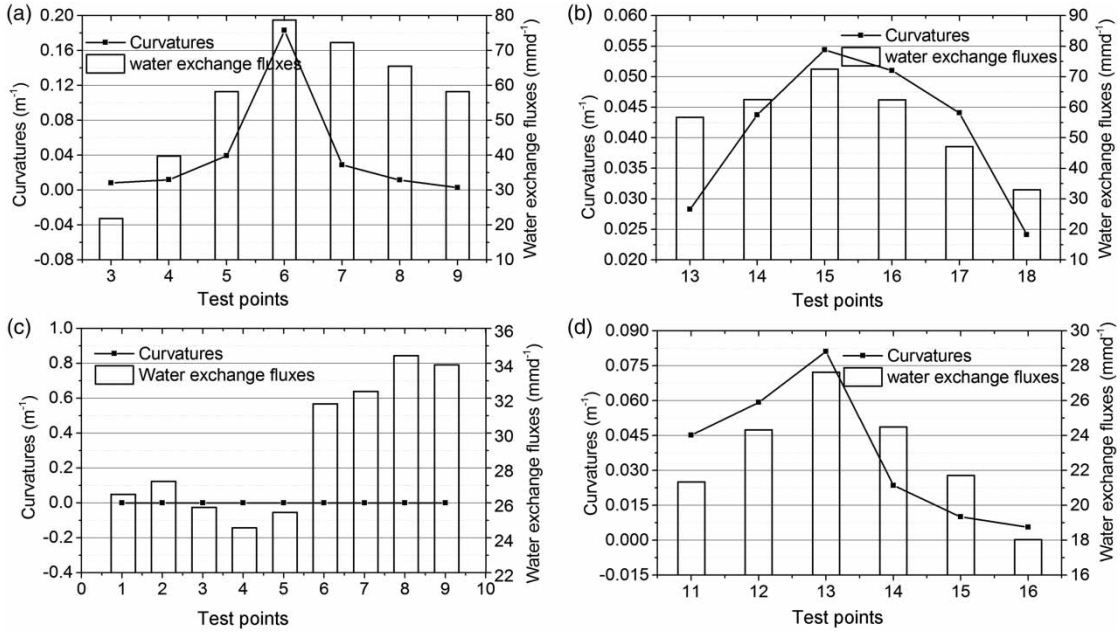

Figure 9 | Curvatures of different test points and hyporheic water exchange fluxes in January 2015 (a), (b) and in July 2015 (c), (d).

variations of sediment test layers as variations of the bank curvatures (Figures 7 and 8). It demonstrated that the curvatures of test points along the bank could possibly act as a driving force of hyporheic water exchange to affect the temperature distributions and vertical water exchange fluxes in the HZ. Additionally, the obvious high temperature of test layers in the DA indicated high water exchange fluxes as well (Figure 7(a)). The results showed that the spatial heterogeneity of sediment vertical layers easily led to the higher magnitudes of vertical hyporheic water exchange. Accordingly, the curvatures of test points and heterogeneity of sediment vertical layers are considered as the crucially important influencing factors for vertical hyporheic water exchange.

Identification of riparian vegetation distributions along the bank

The respective temperature variations of sediment test layers varied little along SB_1 and SB_2 (Figure 8(a)). On the other hand, the temperatures of test layers were significantly lower along SB_2. The curvatures of straight bank segmentations (SB_1 and SB_2) were regarded as the ideal zero in comparison to the meandering bank (Figure 9(c)). However, the significant different magnitudes of vertical hyporheic water exchange occurred in the two different river bank segmentations. For SB_1 or SB_2, the respective magnitudes of vertical water exchange for the test points were almost the same by the analyzation of the corresponding standard deviations (Table 1), but the much higher magnitudes of vertical hyporheic water exchange occurred significantly in SB_2 (Figure 8).

The distances from the bounding of the riparian vegetation region to the bank/water interface, as well as coverage rates and species of arbor, shrub, and herb, are listed in Table 2. Strikingly different distances are demonstrated (Figure 10 and Table 2). In addition, in SB_2 riparian vegetation containing more *willows* was close to the bank/water interface, which accounted for the larger coverage rates compared to SB_1 (Figure 10 and Table 2). The same vertical upward water exchange patterns were presented for nine test points along the straight bank in July 2015 (Figure 6(c)). However, the mean magnitude of vertical water exchange fluxes in SB_2 was higher than that in SB_1 (Table 1), which might have been induced by riparian vegetation distributions in the near-stream system (Williams 1993; Brunke & Gonser 1997; Song *et al.* 2015a). Tabacchi *et al.* (2000) explained the transpiration of riparian

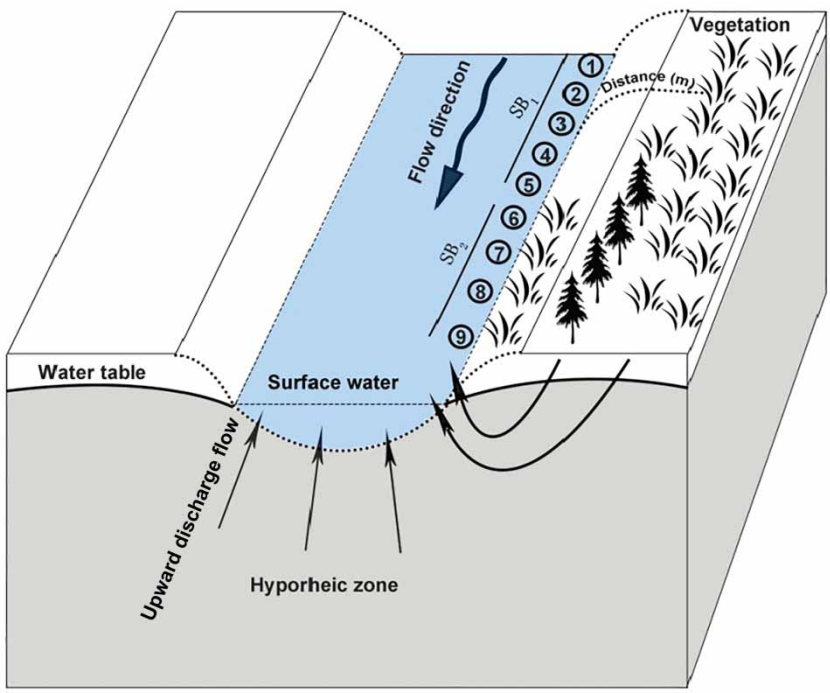

Figure 10 | Schematic map showing test points, riparian vegetation, hyporheic water exchange pattern, and distances from bank/water interface to riparian vegetation for the test period of July 2015.

vegetation was inclined to induce a lower water table during a certain time period, and then greater penetration of the stream into the bank aquifer as a storage bank, which could be applied to discharge the stream during another time period. Compared to the meandering bank in CB_3, which was away from the riparian vegetation regions, the higher vertical water exchange fluxes occurred in the two straight bank segmentations (SB_1 and SB_2) (Figure 8(b)). Accordingly, the fluxes along the straight bank segmentations could possibly be affected by riparian vegetation with the characteristics of water storage (Tabacchi *et al.* 2000), and the flow pattern from the river bank discharging into the stream potentially occurred at the study site (Figure 10). Additionally, the magnitudes of vertical water exchange fluxes in SB_2 were strikingly higher than in SB_1 (Table 1 and Figure 8(b)). The significantly different water exchange fluxes indicated that the water exchange fluxes were mainly affected by the bank storage due to the riparian vegetation (Figures 9(c) and 10). Therefore, on the basis of the upward flow and different vertical water exchange fluxes affected by bank storage, the magnitudes of water exchange fluxes from the river bank discharging into the stream were inferred to be higher in SB_2 than in SB_1. Besides, the alluvial river bank as shown in Figure 10, acting as a reservoir vessel, can impel water discharge into the stream after a short residence period to maintain an equilibrium state between surface water and groundwater. Consequently, during the campaign in July 2015, the water flow pattern from river bank discharging into stream potentially occurred in the study area, and the river bank segmentations (SB_2), with the characteristics of more riparian vegetation adjacent to the bank/water interface, had a larger water discharge capacity in the HZ. Furthermore, the near-stream interactions in the HZ could create a mild habitat for macroinvertebrates and fish by controlling or moderating temperature change (Arrigoni *et al.* 2008), and are significant in maintaining the river's state of health (Song *et al.* 2015a).

In fact, both horizontal and vertical water exchanges are two important components that should be considered. This study focused on vertical hyporheic water exchange. This is a limitation to demonstrating the effect of bank curvatures and riparian vegetation on hyporheic water exchange. The comprehensive effects on hyporheic water exchange

resulting from bank curvatures and riparian vegetation should be demonstrated in further study.

CONCLUSIONS

In this study, the effect of bank curvatures on hyporheic water exchange are determined and discussed at meter scale along the convex banks and straight bank segmentations. The thermal method was applied to determine the patterns and magnitudes of the vertical hyporheic water exchange along the banks in January and July 2015. The results demonstrate that vertical hyporheic water exchange patterns of all test points were upward during the two test periods, and the higher vertical water exchange fluxes mostly occurred in January 2015.

The two convex banks (CB_1 and CB_2) in January 2015 and one convex bank (CB_3) in July 2015 are fitted by establishing the coordinate system to obtain the three corresponding fitting mathematical equations, respectively. The curvatures of different test points along three convex banks are calculated, and then their influences on vertical hyporheic water exchange are discussed and analyzed at meter scale. By comparing the curvatures of different test points along either side of the convex banks, the larger curvatures easily resulted in higher magnitudes of vertical hyporheic water exchange. Additionally, the higher vertical water exchange fluxes significantly occurred near the apex of bends.

The different temperature distributions and vertical water exchange fluxes of the streambed sediment were presented along two segmentations of straight bank (SB_1 and SB_2), although these curvatures were regarded as the idealized zero. The higher vertical water exchange fluxes occurred in SB_2. Due to larger coverage rates of riparian vegetation adjacent to the bank/water interface, the SB_2 site had a larger water discharge capacity in the HZ and was inclined to facilitate the hyporheic flows discharging into the stream to maintain an equilibrium state in the surface–groundwater system.

This study only demonstrates the vertical hyporheic water exchange fluxes. In further study, the other directional flow patterns and magnitudes of hyporheic water exchange should be illustrated as well. It is, therefore, urgent to comprehensively investigate the hyporheic water exchange in all directions along different topographies of the Weihe River based on advanced methodologies.

ACKNOWLEDGEMENTS

This study was jointly supported by the National Natural Science Foundation of China (Grant Nos 51379175 and 51079123), Specialized Research Fund for the Doctoral Program of Higher Education (Grant No. 20136101110001), Program for Key Science and Technology Innovation Team in Shaanxi Province (Grant No. 2014KCT-27) and the Hundred Talents Project of the Chinese Academy of Sciences (Grant No. A315021406). We would like to thank the editor, the associate editor, and the anonymous reviewers for their constructive comments.

REFERENCES

Anderson, M. P. 2005 Heat as a ground water tracer. *Groundwater* **43** (6), 951–968.

Anibas, C., Fleckenstein, J. H., Volze, N., Buis, K., Verhoeven, R., Meire, P. & Batelaan, O. 2009 Transient or steady-state? Using vertical temperature profiles to quantify groundwater-surface water exchange. *Hydrol. Process.* **23** (15), 2165–2177.

Anibas, C., Buis, K., Verhoeven, R., Meire, P. & Batelaan, O. 2011 A simple thermal mapping method for seasonal spatial patterns of groundwater–surface water interaction. *J. Hydrol.* **397** (1), 93–104.

Anibas, C., Verbeiren, B., Buis, K., Chormanski, J., De Doncker, L., Okruszko, T., Meire, P. & Batelaan, O. 2012 A hierarchical approach on groundwater-surface water interaction in wetlands along the upper Biebrza River, Poland. *Hydrol. Earth Syst. Sci.* **16** (7), 2329–2346.

Anibas, C., Schneidewind, U., Vandersteen, G., Joris, I., Seuntjens, P. & Batelaan, O. 2015 From streambed temperature measurements to spatial-temporal flux quantification: using the LPML method to study groundwater–surface water interaction. *Hydrol. Process.* **30** (2), 203–216.

Arriaga, M. A. & Leap, D. I. 2004 Using solver to determine vertical groundwater velocities by temperature variations, Purdue University, Indiana, USA. *Hydrol. J.* **14** (1–2), 253–263.

Arrigoni, A. S., Poole, G. C., Mertes, L. A., O'Daniel, S. J., Woessner, W. W. & Thomas, S. A. 2008 Buffered, lagged, or cooled? Disentangling hyporheic influences on temperature cycles in stream channels. *Water Resour. Res.* **44** (9), W09418.

Bai, Y. C. 2012 Instability of laminar flow in narrow and deep meander channel with constant curvature. *Scientia Sinica Physica, Mechanica & Astronomica* **42** (2), 162–171.

Boano, F., Camporeale, C., Revelli, R. & Ridolfi, L. 2006 Sinuosity-driven hyporheic exchange in meandering rivers. *Geophys. Res. Lett.* **33** (18), 18401–18404.

Boano, F., Revelli, R. & Ridolfi, L. 2007 Bedform-induced hyporheic exchange with unsteady flows. *Adv. Water Res.* **30** (1), 148–156.

Boyraz, U. & Kazezyılmaz-Alhan, C. M. 2014 An investigation on the effect of geometric shape of streams on stream/ground water interactions and ground water flow. *Hydrol. Res.* **45** (4–5), 575–588.

Brunke, M. & Gonser, T. 1997 The ecological significance of exchange processes between rivers and groundwater. *Freshwater Biol.* **37** (1), 1–33.

Cai, Y., Huang, W. R., Teng, F., Wang, B. B., Ni, K. & Zheng, C. M. 2015 Spatial variations of river–groundwater interactions from upstream mountain to midstream oasis and downstream desert in Heihe River basin, China. *Hydrol. Res.* **47** (1), nh2015072.

Cardenas, M. B. 2009 Stream–aquifer interactions and hyporheic exchange in gaining and losing sinuous streams. *Water Resour. Res.* **45** (6), W06429.

Cardenas, M. B. & Wilson, J. 2006 The influence of ambient groundwater discharge on exchange zones induced by current–bedform interactions. *J. Hydrol.* **331** (1), 103–109.

Cardenas, M. B., Wilson, J. & Zlotnik, V. A. 2004 Impact of heterogeneity, bed forms, and stream curvature on subchannel hyporheic exchange. *Water Resour. Res.* **40** (8), W08307(08301-08313).

Carey, S. & Quinton, W. 2005 Evaluating runoff generation during summer using hydrometric, stable isotope and hydrochemical methods in a discontinuous permafrost alpine catchment. *Hydrol. Process.* **19** (1), 95–114.

Cheng, D. H., Wang, Y. H., Duan, J. B., Chen, X. H. & Yang, S. K. 2015 A new analytical expression for ultimate specific yield and shallow groundwater drainage. *Hydrol. Process.* **29** (8), 1905–1911.

Cranswick, R. H. & Cook, P. G. 2015 Scales and magnitude of hyporheic, river–aquifer and bank storage exchange fluxes. *Hydrol. Process.* **29** (14), 3084–3097.

Cranswick, R. H., Cook, P. G. & Lamontagne, S. 2014 Hyporheic zone exchange fluxes and residence times inferred from riverbed temperature and radon data. *J. Hydrol.* **519** (Part B), 1870–1881.

Datry, T., Larned, S. T. & Scarsbrook, M. R. 2007 Responses of hyporheic invertebrate assemblages to large-scale variation in flow permanence and surface–subsurface exchange. *Freshwater Biol.* **52** (8), 1452–1462.

Fanelli, R. M. & Lautz, L. K. 2008 Patterns of water, heat, and solute flux through streambeds around small dams. *Groundwater* **46** (5), 671–687.

Fleckenstein, J. H., Krause, S., Hannah, D. M. & Boano, F. 2010 Groundwater-surface water interactions: new methods and models to improve understanding of processes and dynamics. *Adv. Water Res.* **33** (11), 1291–1295.

Gomez-Velez, J. D., Harvey, J. W., Cardenas, M. B. & Kiel, B. 2015 Denitrification in the Mississippi River network controlled by flow through river bedforms. *Nat. Geosci.* **8** (12), 941–945.

Hatch, C. E., Fisher, A. T., Revenaugh, J. S., Constantz, J. & Ruehl, C. 2006 Quantifying surface water–groundwater interactions using time series analysis of streambed thermal records: method development. *Water Resour. Res.* **42** (10), W10410 (10411-10414).

Jiang, W. W., Song, J. X., Zhang, J. L., Wang, Y. Y., Zhang, N., Zhang, X. H., Long, Y. Q., Li, J. X. & Yang, X. G. 2015 Spatial variability of streambed vertical hydraulic conductivity and its relation to distinctive stream morphologies in the Beiluo River, Shaanxi Province, China. *Hydrol. J.* **23** (7), 1617–1626.

Jin, G. Q., Tang, H. W., Gibbes, B., Li, L. & Barry, D. A. 2010 Transport of nonsorbing solutes in a streambed with periodic bedforms. *Adv. Water Res.* **33** (11), 1402–1416.

Jin, G. Q., Tang, H. W., Li, L. & Barry, D. A. 2011 Hyporheic flow under periodic bed forms influenced by low-density gradients. *Geophys. Res. Lett.* **38** (22), L22401.

Kalbus, E., Reinstorf, F. & Schirmer, M. 2006 Measuring methods for groundwater–surface water interactions: a review. *Hydrol. Earth Syst. Sci.* **10** (6), 873–887.

Krause, S., Hannah, D. & Fleckenstein, J. 2009 Hyporheic hydrology: interactions at the groundwater–surface water interface. *Hydrol. Process.* **23** (15), 2103–2107.

Li, B. D., Zhang, X. H., Xu, C. Y., Zhang, H. & Song, J. X. 2015 Water balance between surface water and groundwater in the withdrawal process: a case study of the Osceola watershed. *Hydrol. Res.* **46** (6), 943–953.

Lowry, C. S., Walker, J. F., Hunt, R. J. & Anderson, M. P. 2007 Identifying spatial variability of groundwater discharge in a wetland stream using a distributed temperature sensor. *Water Resour. Res.* **43** (10), W10408.

Malard, F., Tockner, K., Dole-Olivier, M. J. & Ward, J. 2002 A landscape perspective of surface–subsurface hydrological exchanges in river corridors. *Freshwater Biol.* **47** (4), 621–640.

Naranjo, R. C. & Turcotte, R. 2015 A new temperature profiling probe for investigating groundwater–surface water interaction. *Water Resour. Res.* **51** (9), 7790–7797.

Nowinski, J. D., Cardenas, M. B. & Lightbody, A. F. 2011 Evolution of hydraulic conductivity in the floodplain of a meandering river due to hyporheic transport of fine materials. *Geophys. Res. Lett.* **38** (1), L01401–L01405.

Revelli, R., Boano, F., Camporeale, C. & Ridolfi, L. 2008 Intra-meander hyporheic flow in alluvial rivers. *Water Resour. Res.* **44** (12).

Şahin, A. U. & Çiftçi, E. 2016 An area matching process to estimate the hydraulic parameters using transient constant-head test data. *Hydrol. Res.* **47** (1), nh2016132.

Schmidt, C., Bayer-Raich, M. & Schirmer, M. 2006 Characterization of spatial heterogeneity of groundwater-stream water interactions using multiple depth streambed

temperature measurements at the reach scale. *Hydrol. Earth Syst. Sci. Discuss.* **3** (4), 1419–1446.

Schmidt, C., Conant Jr, B., Bayer-Raich, M. & Schirmer, M. 2007 Evaluation and field-scale application of an analytical method to quantify groundwater discharge using mapped streambed temperatures. *J. Hydrol.* **347** (3), 292–307.

Schmidt, C., Büttner, O., Musolff, A. & Fleckenstein, J. H. 2014 A method for automated, daily, temperature-based vertical streambed water-fluxes. *Fundamental and Applied Limnology/Archiv für Hydrobiologie* **184** (3), 173–181.

Shope, C. L., Constantz, J. E., Cooper, C. A., Reeves, D. M., Pohll, G. & McKay, W. A. 2012 Influence of a large fluvial island, streambed, and stream bank on surface water-groundwater fluxes and water table dynamics. *Water Resour. Res.* **48** (6), 1–18.

Song, J. X., Cheng, D. D., Li, Q., He, X. J., Long, Y. Q. & Zhang, B. 2015a An evaluation of river health for the Weihe River in Shaanxi Province. *China. Adv. Meteorol.* **2015**, 1–13.

Song, J. X., Yang, X. G., Zhang, J. L., Long, Y. Q., Zhang, Y. & Zhang, T. F. 2015b Assessing the variability of heavy metal concentrations in liquid-solid two-phase and related environmental risks in the Weihe River of Shaanxi Province, China. *Int. J. Environ. Res. Public Health* **12** (7), 8243–8262.

Stallman, R. 1965 Steady one-dimensional fluid flow in a semi-infinite porous medium with sinusoidal surface temperature. *J. Geophys. Res.* **70** (12), 2821–2827.

Stonedahl, S. H., Harvey, J. W., Wörman, A., Salehin, M. & Packman, A. I. 2010 A multiscale model for integrating hyporheic exchange from ripples to meanders. *Water Resour. Res.* **46** (12), W12539.

Stonedahl, S. H., Harvey, J. W. & Packman, A. I. 2013 Interactions between hyporheic flow produced by stream meanders, bars, and dunes. *Water Resour. Res.* **49** (9), 5450–5461.

Storey, R. G., Howard, K. W. F. & Williams, D. D. 2003 Factors controlling riffle-scale hyporheic exchange flows and their seasonal changes in a gaining stream: a three-dimensional groundwater flow model. *Water Resour. Res.* **39** (2), 1034.

Suzuki, S. 1960 Percolation measurements based on heat flow through soil with special reference to paddy fields. *J. Geophys. Res.* **65** (9), 2883–2885.

Tabacchi, E., Lambs, L., Guilloy, H., Planty-Tabacchi, A. M., Muller, E. & Decamps, H. 2000 Impacts of riparian vegetation on hydrological processes. *Hydrol. Process.* **14** (16–17), 2959–2976.

Tan, Z. Q., Zhang, Q., Li, M. F., Li, Y. L., Xu, X. L. & Jiang, J. H. 2016 A study of the relationship between wetland vegetation communities and water regimes using a combined remote sensing and hydraulic modeling approach. *Hydrol. Res.* **47** (S1), 278–292.

Wei, S. K., Song, J. X. & Khan, N. I. 2012 Simulating and predicting river discharge time series using a wavelet-neural network hybrid modelling approach. *Hydrol. Process.* **26** (2), 281–296.

Williams, D. D. 1993 Nutrient and flow vector dynamics at the hyporheic/groundwater interface and their effects on the interstitial fauna. *Hydrobiologia* **251** (1–3), 185–198.

Wörman, A., Packman, A. I., Johansson, H. & Jonsson, K. 2002 Effect of flow-induced exchange in hyporheic zones on longitudinal transport of solutes in streams and rivers. *Water Resour. Res.* **38** (1), 2-1–2-15.

Wörman, A., Packman, A. I., Marklund, L., Harvey, J. W. & Stone, S. H. 2006 Exact three-dimensional spectral solution to surface–groundwater interactions with arbitrary surface topography. *Geophys. Res. Lett.* **33** (7), 7402(7401-7404).

Yuan, D. K., Lin, B. L. & Falconer, R. 2008 Simulating moving boundary using a linked groundwater and surface water flow model. *J. Hydrol.* **349** (3), 524–535.

Zhu, T. Y., Fu, D. F., Jenkinson, B. & Jafvert, C. T. 2015 Calibration and application of an automated seepage meter for monitoring water flow across the sediment-water interface. *Environ. Monit. Assess.* **187** (4), 1–11.

Zuo, D. P., Xu, Z. X., Wu, W., Zhao, J. & Zhao, F. F. 2014 Identification of streamflow response to climate change and human activities in the Wei River Basin, China. *Water Resour. Manage.* **28** (3), 833–851.

First received 30 January 2016; accepted in revised form 25 April 2016. Available online 6 June 2016